






Article

Evaluation of Semi-Analytical Algorithms to Retrieve Particulate and Dissolved Absorption Coefficients in Gulf of California Optically Complex Waters

Stella Patricia Betancur-Turizo ^{1,2} , Adriana González-Silvera ^{1,*} ,
Eduardo Santamaría-del-Ángel ¹ , Jing Tan ³  and Robert Frouin ³ 

- ¹ Facultad de Ciencias Marinas, Universidad Autónoma de Baja California, Carretera Tijuana-Ensenada Km 103, 22800 Ensenada, BC, México; sbetancur@dimar.mil.co (S.P.B.-T.); santamaria@uabc.edu.mx (E.S.d.-A.)
² Centro de Investigaciones Oceanográficas e Hidrográficas del Caribe, Área de Protección del Medio Marino, Barrio Bosque, Sector Manzanillo, Cartagena de Indias, Cartagena 130001, Bolívar, Colombia
³ Scripps Institution of Oceanography, University of California San Diego, La Jolla, California, CA 92093, USA; jtit079@ucsd.edu (J.T.); rfrouin@ucsd.edu (R.F.)
 * Correspondence: adriana.gonzalez@uabc.edu.mx; Tel.: +52-646-151-0574

Received: 27 July 2018; Accepted: 31 August 2018; Published: 10 September 2018



Abstract: Two semi-analytical algorithms, Generalized Inherent Optical Property (GIOP) and Garver-Siegel-Maritorena (GSM), were evaluated in terms of how well they reproduced the absorption coefficient of phytoplankton ($a_{ph}(\lambda)$) and dissolved and detrital organic matter ($a_{dg}(\lambda)$) at three wavelengths (λ of 412, 443, and 488 nm) in a zone with optically complex waters, the Upper Gulf of California (UGC) and the Northern Gulf of California (NGC). In the UGC, detritus determines most of the total light absorption, whereas, in the NGC, chromophoric dissolved organic material (CDOM) and phytoplankton dominate. Upon comparing the results of each model with a database assembled from four cruises done from spring to summer (March through September) between 2011 and 2013, it was found that GIOP is a better estimator for $a_{ph}(\lambda)$ than GSM, independently of the region. However, both algorithms underestimate in situ values in the NGC, whereas they overestimate them in the UGC. Errors are associated with the following: (a) the constant $a^*_{ph}(\lambda)$ value used by GSM and GIOP ($0.055 \text{ m}^2 \text{ mgChl}a^{-1}$) is higher than the most frequent value observed in this study's data ($0.03 \text{ m}^2 \text{ mgChl}a^{-1}$), and (b) satellite-derived chlorophyll *a* concentration (Chl*a*) is biased high compared with in situ Chl*a*. GIOP gave also better results for the $a_{dg}(\lambda)$ estimation than GSM, especially in the NGC. The spectral slope S_{dg} was identified as an important parameter for estimating $a_{dg}(\lambda)$, and this study's results indicated that the use of a fixed input value in models was not adequate. The evaluation confirms the lack of generality of algorithms like GIOP and GSM, whose reflectance model is too simplified to capture expected variability. Finally, a greater monitoring effort is suggested in the study area regarding the collection of in situ reflectance data, which would allow explaining the effects that detritus and CDOM may have on the semi-analytical reflectance inversions, as well as isolating the possible influence of the atmosphere on the satellite-derived water reflectance and Chl*a*.

Keywords: ocean color; inherent optical properties; remote sensing

1. Introduction

Ocean color remote sensors onboard satellites, such as the early coastal zone color scanner (CZCS) and the current Moderate Resolution Imaging Spectroradiometer (MODIS), have provided information on oceanographic structures and processes at different scales in the oceans, explaining a series of

biological and ecological processes [1]. The data from these sensors has been used in studies on ocean dynamics, biogeochemistry, and global climate change [2–5].

Specifically, these sensors have greatly improved the world's understanding of the properties of light absorption by water and particulate and dissolved material [6–12], and they have emphasized the importance of observing the properties routinely from space. These properties exercise an important influence on the function of marine ecosystems, determining, for example, the availability of solar radiation for phytoplankton growth [13], the effectiveness of visual predation [14], and the kinetics of photochemical processes [15].

The concentration of particulate material in water is important in coastal regions, with implications for coastal protection, shipping, and recreational activities [16]. The analysis of absorption is necessary for identifying the water components that contribute to the process of light absorption. The total absorption can be described in terms of the additive contribution of different components [17]:

$$a(\lambda) = a_w(\lambda) + a_p(\lambda) + a_{CDOM}(\lambda) \quad (1)$$

where $a(\lambda)$ is the light absorption coefficient at a given wavelength; $a_w(\lambda)$ is the light absorption coefficient by pure water; $a_p(\lambda)$ is the light absorption coefficient by particulate material, which in turn can be decomposed into the absorption by phytoplankton ($a_{ph}(\lambda)$) and the absorption by detrital organic particles and minerals ($a_d(\lambda)$); and, finally, $a_{CDOM}(\lambda)$ is the absorption coefficient by chromophoric dissolved organic material (CDOM). The coefficients $a_d(\lambda)$ and $a_{CDOM}(\lambda)$ have similar spectral shapes and they are evaluated as a sum ($a_{dg}(\lambda)$) [16]. Therefore, the total absorption $a(\lambda)$ can also be expressed as follows:

$$a(\lambda) = a_w(\lambda) + a_{ph}(\lambda) + a_{dg}(\lambda) \quad (2)$$

The absorption coefficients ($a_{ph}(\lambda)$, $a_{dg}(\lambda)$) and the particulate backscattering coefficient ($b_{bp}(\lambda)$) are referred to as inherent optical properties (IOPs) [18], and a variety of semi-analytical approaches have been proposed [16] to derive IOPs from the remotely measured “remote-sensing” spectral reflectance ($R_{rs}(\lambda)$) [19], especially for optically complex waters [20]. Two well-known—and widely used—semi-analytical algorithms have been proposed by Maritorena et al. [21] and Werdell et al. [22]. The first algorithm, known as Garver-Siegel-Maritorena (GSM), was initially developed by Garver and Siegel [6] and it is based on a quadratic relationship between $R_{rs}(\lambda)$ and the absorption and scattering coefficients [23]. It uses a semi-analytical approach and an optimization method to obtain estimates of chlorophyll *a* concentration (Chl*a*), $a_{dg}(443)$, and $b_{bp}(443)$, assuming an underlying bio-optical model and using non-linear optimization [16]. The GSM products generated by NASA's Ocean Biology Processing Group (OBPG) are described at <https://oceancolor.gsfc.nasa.gov/products/eval/#GSM>. The second algorithm, referred to as Generalized Inherent Optical Property (GIOP), also uses spectral optimization, but incorporates several ideas from previously published bio-optical models and methods, allowing the user to isolate and evaluate the individual differences between models in a controlled environment. GIOP products are standard NASA OBPG products; see <https://oceancolor.gsfc.nasa.gov/atbd/giop/>. GIOP was developed during two NASA-sponsored international IOP algorithm workshops at the Ocean Optics XIX (October 2008) and XX (September 2010) conferences. The international working group associated with these workshops proposed in consensus the preliminary configuration of GIOP, with alternative settings and characteristics of the model defined with the objective of applying continuous evaluations.

Brewin et al. [16], among others, have evaluated the semi-analytical algorithms available for the determination of IOPs, by means of an objective classification that allowed the grading of each one. Their results showed that the overall score obtained by the algorithms that estimated $a_{ph}(\lambda)$, when accounting for individual scores across all wavelengths, was higher in GIOP, followed by the others, among which was GSM. For the determination of $a_{dg}(\lambda)$, the slightly higher scores obtained were for the Quasi-Analytical Algorithm (QAA) [24,25] and the Hyperspectral Optimization Process Exemplar (HOPE) models [26], followed by other algorithms including GSM and GIOP. Meanwhile,

none of the algorithms captured well the variability in S_{dg} (spectral slope of $a_{dg}(\lambda)$). In their study, the above authors indicated the need to use, in future inter-comparison exercises, an independent in situ dataset for testing algorithms (in this case, NASA bio-Optical Marine Algorithm Dataset, NOMAD).

In this study, the authors evaluated GSM and GIOP by comparing their results with an in situ database of $a_{ph}(\lambda)$, $a_d(\lambda)$, and $a_{CDOM}(\lambda)$ from an optically complex region, the northern part of the Gulf of California. The selection of the best model was done based on statistical tests, and the results of the analyses allowed the authors to identify the possible adaptations of the algorithm that could improve the retrieval in this type of region.

2. Materials and Methods

2.1. Study Area

The study area comprises the northern part of the Gulf of California (Mexico) and is located at 30.5°N to 32°N and −115°W to −113.5°W (see Figure 1). In previous studies, this area has been classified into two zones (Upper Gulf of California and Northern Gulf of California) according to hydrodynamic characteristics and bio-optical properties [27–29]. The shallower zone (<30 m) is the Upper Gulf of California (UGC) and is characterized by high turbidity and strong water-column mixing [30], high chlorophyll *a* concentration (Chl*a*), the dominance of microphytoplankton (diatoms and dinoflagellates), and a high contribution of detritus to total light absorption [29]. The Northern Gulf of California (NGC) is a deeper region more oligotrophic than the UGC, dominated by picophytoplankton (cyanobacteria and green algae), with lower values of Chl*a* and light absorption by detritus [29]. A transitional zone separates both regions (see Figure 1), whose location can change according to differences in hydrodynamics. A detailed description of the particular bio-optical characteristics of each region can be found in Betancur-Turizo et al. [29].

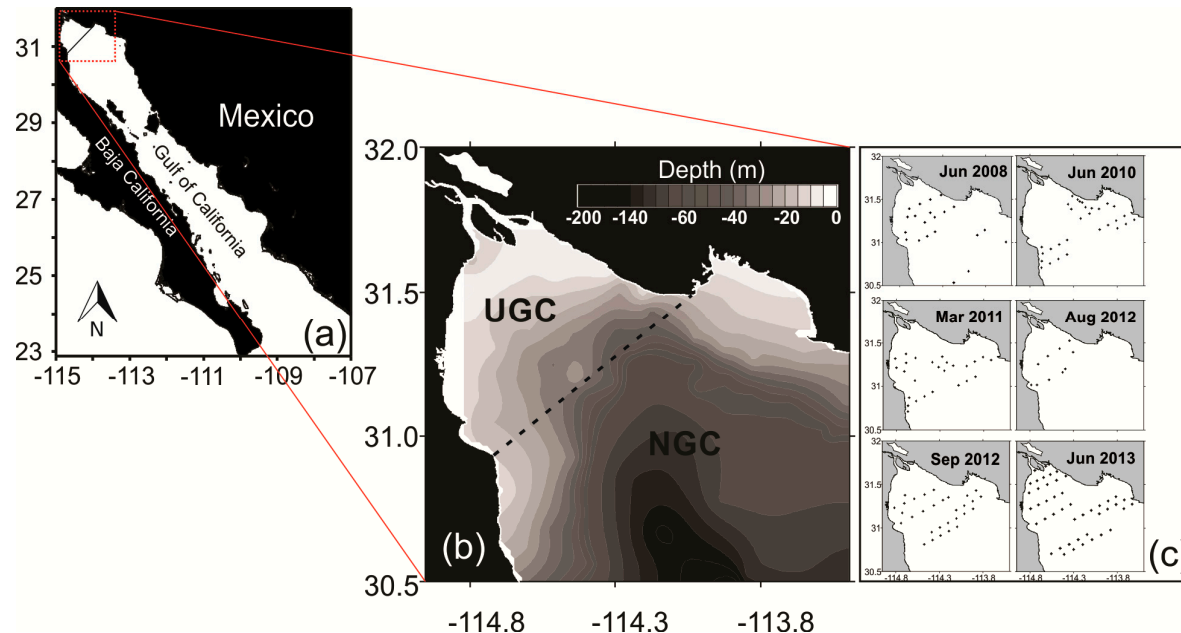


Figure 1. (a) Study area map. (b) Transition zone between the Upper Gulf of California (UGC) and Northern Gulf of California (NGC) bio-optical regions, indicated by the dotted line. (c) Station location for each cruise.

2.2. In Situ Data

Physical and biological data were collected during six oceanographic cruises in the study area performed during neap tides. Table 1 indicates the sampling dates, and Figure 1c the location of the stations. Surface water samples (approximately 0.50 m deep) were collected using 5 L Niskin bottles

for the determination of phytoplankton ($a_{ph}(\lambda)$), detritus ($a_d(\lambda)$), and CDOM ($a_{CDOM}(\lambda)$) absorption coefficients according to the protocol indicated in Mitchell et al. [17]. Chl *a* concentration was measured using High-performance liquid chromatography (HPLC) with the method proposed by Thomas [31]. The specific absorption coefficient by phytoplankton ($a_{ph}^*(\lambda)$, m^2 (mg Chl *a*)^{−1}) was calculated by normalizing $a_{ph}(\lambda)$ by Chl *a*. More details of these analyses are provided in Betancur-Turizo et al. [29].

Table 1. General information of the oceanographic cruises and measured variables.

Cruises	Dates	Variables
June 2008	3–16	$a_{ph}(\lambda)$, $a_d(\lambda)$
June 2010	1–10	$a_{ph}(\lambda)$, $a_d(\lambda)$
March 2011	24 March to 1 April	$a_{ph}(\lambda)$, $a_d(\lambda)$, $a_{CDOM}(\lambda)$
August 2012	3–10	$a_{ph}(\lambda)$, $a_d(\lambda)$, $a_{CDOM}(\lambda)$
September 2012	4–9	$a_{ph}(\lambda)$, $a_d(\lambda)$, $a_{CDOM}(\lambda)$
June 2013	11–21	$a_{ph}(\lambda)$, $a_d(\lambda)$, $a_{CDOM}(\lambda)$

The semi-analytical algorithms that determine the IOPs do not estimate the absorption coefficients of detritus $a_d(\lambda)$ and $a_{CDOM}(\lambda)$ independently, but as an integrated variable called $a_{dg}(\lambda)$ which represents their sum. For this reason, this variable was determined by the sum of each of the absorption spectra of $a_d(\lambda)$ and $a_{CDOM}(\lambda)$. The newly generated spectra were fitted to an exponential function $y = Ae^{(-S*\lambda)}$ between 250 and 500 nm using a nonlinear least square minimization routine. The exponent *S* of the equation was called S_{dg} and corresponds to the spectral slope of the absorption spectrum of $a_{dg}(\lambda)$. Finally, given that the June 2008 and 2010 cruises did not have CDOM data, the analyses of this variable were applied only to the data of the four cruises taken between 2011 and 2013 (see Table 1).

2.3. Satellite Data

A selection process of MODIS-Aqua Level 1A files was done, in which scenes with less than 80% cloudiness and/or sun glint were selected for the study period. The result was a total of 48 images (see Table 2) with a spatial resolution of ~1.1 km at nadir. These files were extracted from the online OBPB Data Processing System database (<https://oceancolor.gsfc.nasa.gov/cgi/browse.pl>) in accordance with the available passes depending on the date of each analyzed cruise (see Table 2).

Table 2. General information on the in situ database analyzed and effective monitoring days used for the extraction of Level 1A images.

Cruises	Total Stations	Julian Days	Total Days Per Cruise	Selected Level 1a Images
June 2008	22	158–164	6	11
June 2010	30	152–159	8	8
March 2011	27	84–91	8	10
August 2012	10	216–223	8	3
September 2012	30	248–253	6	6
June 2013	46	162–171	9	10
Total	165		55	48

For the processing of Level 1A archives to Level 2, the L2GEN program was used and its standard atmospheric correction scheme (SeaDAS version 7.4) was applied, selecting the IOP products $a_{dg}(\lambda)$ and $a_{ph}(\lambda)$ at 412 nm, 443 nm, and 488 nm in their default configuration for algorithms GIOP and GSM. After the generation of the L2 archives, the statistics median, the standard deviation, and the number of valid pixels were calculated.

An exclusion process for each geographical position extracted was applied in those cases for which one or more of the Level 2 L2GEN quality control indicators were not fulfilled (see Table 3). All Level 2 archive variables were extracted from 3 × 3 pixel windows, centered on the pixel closest to the in situ sample. For the analyses, only data with at least three valid pixels (out of a total of nine)

were included, due to increased errors from pixels close to clouds or land. Only model data with quality control were paired with in situ information of the six cruises analyzed (see Figure 2).

Table 3. Level 2 flags used for excluding pixels from analysis.

Name	Description
ATMFAIL	Atmospheric correction failure
HIGLINT	High glint determined
HILT	High (or saturating) Top of the Atmosphere (TOA radiance)
HISATZEN	Large satellite zenith angle
STRAYLIGHT	Stray light determined
CLDICE	Probable cloud or ice contamination
LOWLW	Very low water-leaving radiance
MAXAERITER	Absorbing aerosols determined

The MODIS-Aqua images for match-up analysis (one km spatial resolution) were processed for $Chl a$ estimation using SeaDAS V7 and using the OCx product with the OC3M algorithm. Average $Chl a$ from a box of 3×3 pixels centered at the station position was used for comparison between MODIS $Chl a$ and in situ $Chl a$ in order to evaluate its influence on the $a_{ph}(\lambda)$ estimation.

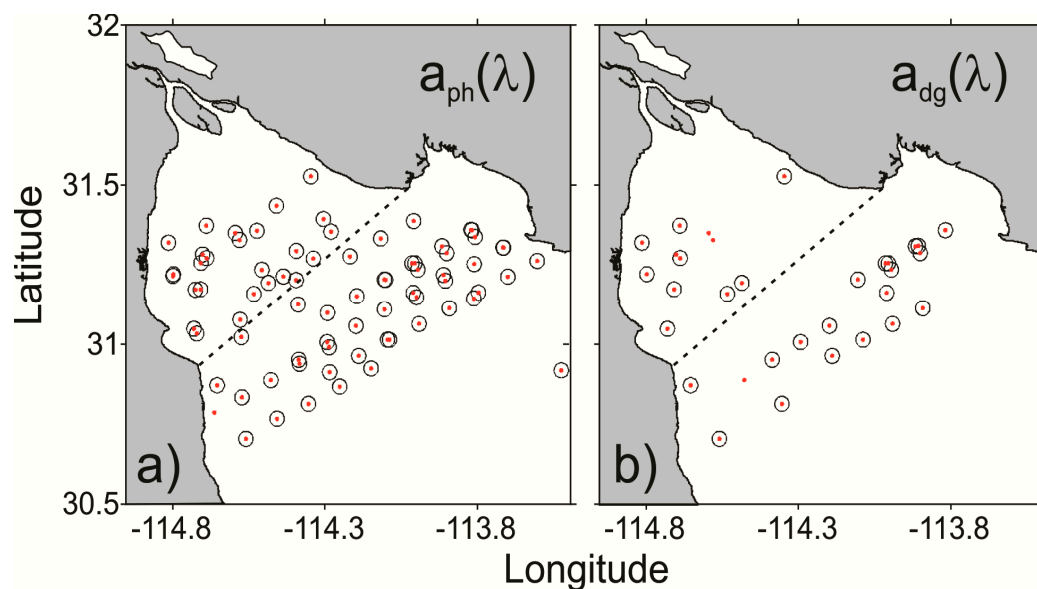


Figure 2. Data of the six cruises that had in situ information on the coefficients (a) $a_{ph}(\lambda)$ and (b) $a_{dg}(\lambda)$ in the study zone. Black circles represent stations paired with the Generalized Inherent Optical Property (GIOP) algorithm, and red points represent stations paired with the Garver-Siegel-Maritorena (GSM) algorithm. The dotted black line represents the intermediate position of the transitional zone that separates the bio-optical regions UGC and NGC [29].

2.4. Semi-Analytical Algorithms

GIOP and GSM were used to retrieve the absorption coefficients from the satellite data, and the estimates were compared with in situ data. In GSM [21], the following parameterizations are used:

$$a_{ph}(\lambda) = Chl a \ a_{ph}(\lambda) \quad (3)$$

$$a_{dg}(\lambda) = a_{dg}(443) \exp^{-S(\lambda-443)} \quad (4)$$

A constant value for $a_{ph}^*(\lambda)$ is specified as $0.055 \text{ m}^2 \text{ mgChl } a^{-1}$. S is the spectral decay constant for dissolved substances and detritus absorption [32], whose value has been specified in the GSM source

code as $S_{dg} = 0.02061 \text{ nm}^{-1}$ [33]. Using the spectral satellite radiance as input, the Levenberg-Marquadt nonlinear least squares procedure was employed to solve for the remaining unknown terms, namely $Chla$ and $a_{dg}(\lambda)$ [32].

GIOP uses the same constant value for $a_{ph}^*(\lambda)$ ($0.055 \text{ m}^2 \text{ mgChla}^{-1}$) that is used in GSM, although S_{dg} is specified as 0.018 nm^{-1} . The GIOP model [22] allows one to specify different parameterizations and optimization approaches, including the $a_{ph}^*(\lambda)$ and S_{dg} eigenvectors employed, the number of eigenvalues resolved, the optimization method selected, and the number of sensor wavelengths. All of these GIOP elements are therefore defined by specifying eigenvectors for each optically significant constituent assumed to exist in the water column [22].

2.5. Algorithm Evaluation Methodology

The degree of association between the IOP products and the in situ data was evaluated through the “match-up” technique [34]. Variables graphed were the absorption coefficient of phytoplankton ($a_{ph}(412, 443, \text{ and } 488)$) and the absorption coefficient of CDOM and detritus ($a_{dg}(412, 443, \text{ and } 488)$) (y axis) against their respective in situ counterparts (x axis). These wavelengths were selected because they are representative of most remote sensors and in particular MODIS-Aqua. Below are the statistics that were used for the algorithm evaluation.

Pearson’s Correlation Coefficient (r_p)

The statistical validity of the models was determined through the Pearson’s correlation coefficient (r_p), whose mathematical expression is as follows [35]:

$$r_p = \frac{Cov_{A,B}}{(SD_A \times SD_B)}, \quad (5)$$

where $Cov_{A,B}$ is the covariance of A and B and SD_A and SD_B are the standard deviation of A and B . This coefficient is a measure of the correlation (linear dependence) between two variables A and B , giving a value between $+1$ and -1 inclusive (1 indicates a direct linear relationship, -1 indicates an inverse linear correlation, and zero indicates no linear relationship). The coefficient’s significance is determined with a hypothesis test, known as correlation analysis [35]:

$$H_0: r_p = 0, \quad (6)$$

$$H_a: r_p \neq 0. \quad (7)$$

To accept or reject hypothesis H_0 , the value $r_{\text{calculated}}$ was compared with the value r_{critical} based on the degree of freedom ($df = n - 1$) and the error α (0.05). r_{critical} was the minimum significant value of r_p . If $r_{\text{calculated}} > r_{\text{critical}}$, H_0 was rejected and r_p was statistically significant, but if $r_{\text{calculated}} < r_{\text{critical}}$, H_0 could not be rejected and r_p was not significant [34].

Root Mean Square Error (RMSE)

The Root Mean Square Error (RMSE) is a frequently used measure of the difference between values predicted by a model (x_i = satellite data) and the values actually observed (y_i = in situ data) from the environment that is being modeled. It is calculated according to [35]:

$$RMSE = \sqrt{\frac{1}{N} \sum_{i=1}^N (y_i - x_i)^2} \quad (8)$$

The RMSE can be confirmed using the sum of square errors (χ^2): this statistical test is the minimum error of the modeled data (satellite) with respect to the observed data (in situ). In the comparison

between models, the lesser value of χ^2 is the one which better describes the answer and is calculated according to [35]:

$$\chi^2 = \sum (y - \hat{y})^2 \quad (9)$$

Bias

Bias provides information on the tendency of the model to overestimate (Bias > 0) or underestimate (Bias < 0) a variable and is calculated according to [35]:

$$\text{Bias} = \frac{1}{N} \sum_{i=1}^N \left(\frac{y_i - x_i}{x_i} \right) \quad (10)$$

Taylor Diagram

The Taylor diagram illustrates a different set of statistics in terms of $u\text{RMSD}^*$ that is comprised of the standard deviation (σ) of the model output and in situ data, σ_{model} and $\sigma_{\text{in situ}}$, as well as the Pearson's correlation coefficient (r_p) between estimates and in situ measurements [36]:

$$u\text{RMSD}^* = \sqrt{1 + \frac{\sigma_{\text{model}}^2}{\sigma_{\text{in situ}}^2} - 2 * \frac{\sigma_{\text{model}}}{\sigma_{\text{in situ}}} * r_p} \quad (11)$$

The Taylor diagram provides a way of 2-D graphing three statistical parameters (r_p , σ , and RMSE) that indicate how closely a pattern matches observations. With these statistics in the same plot, it is easy to determine how much of the overall root-mean-square difference in patterns is attributable to a difference in variance and how much is due to poor pattern correlation [37]. The statistical significance was evaluated using an α of 5%.

3. Results and Discussion

3.1. Phytoplankton Absorption Coefficient

Betancur-Turizo et al. [29] analyzed the spatial and temporal variability of light absorption properties in the study area. They observed that there was a strong temporal variability with a spatial pattern that allowed the definition of two bio-optical regions named Upper Gulf of California (UGC) and Northern Gulf of California (NGC), with particular characteristics that indicated that these regions were very different when evaluating the individual contribution by phytoplankton, detritus, and CDOM to total light absorption. In particular, in the UGC, $a_d(\lambda)$ contribution to total light absorption was most of the time higher than 40% followed by $a_{\text{CDOM}}(\lambda)$, whereas in the NGC, a co-dominium between $a_{\text{ph}}(\lambda)$ and $a_{\text{CDOM}}(\lambda)$ was observed most of the time.

In this study, a total of 150 a_{ph} (412, 443, and 448) in situ data were collected, but because of clouds, atmospheric corrections failure, and other aspects described in Table 3, only 75 match-ups were generated for GIOP and 76 for GSM (see Figure 2a). The difference in the number of data used for GIOP and GSM was due to outliers that were excluded from the analysis. The data used for these analyses are listed in the Supplementary Material (see Table S1). Figure 3 presents the comparison between the in situ data and the algorithm output for the entire dataset and also by region (UGC and NGC). The performance statistics indicated that GIOP was in general a better $a_{\text{ph}}(\lambda)$ estimator than GSM regardless of the bio-optical region, although the differences were small. Special attention should be given to the strong underestimation of $a_{\text{ph}}(412)$ by GSM, independently of the bio-optical region (bias between -0.70 to -0.86) (see Figure 3d–f). However, both algorithms in general underestimated the in situ values (negative bias) in the NGC, whereas they overestimated them (positive bias) in the UGC, although the negative bias in the NGC was much lower than the positive ones in the UGC.

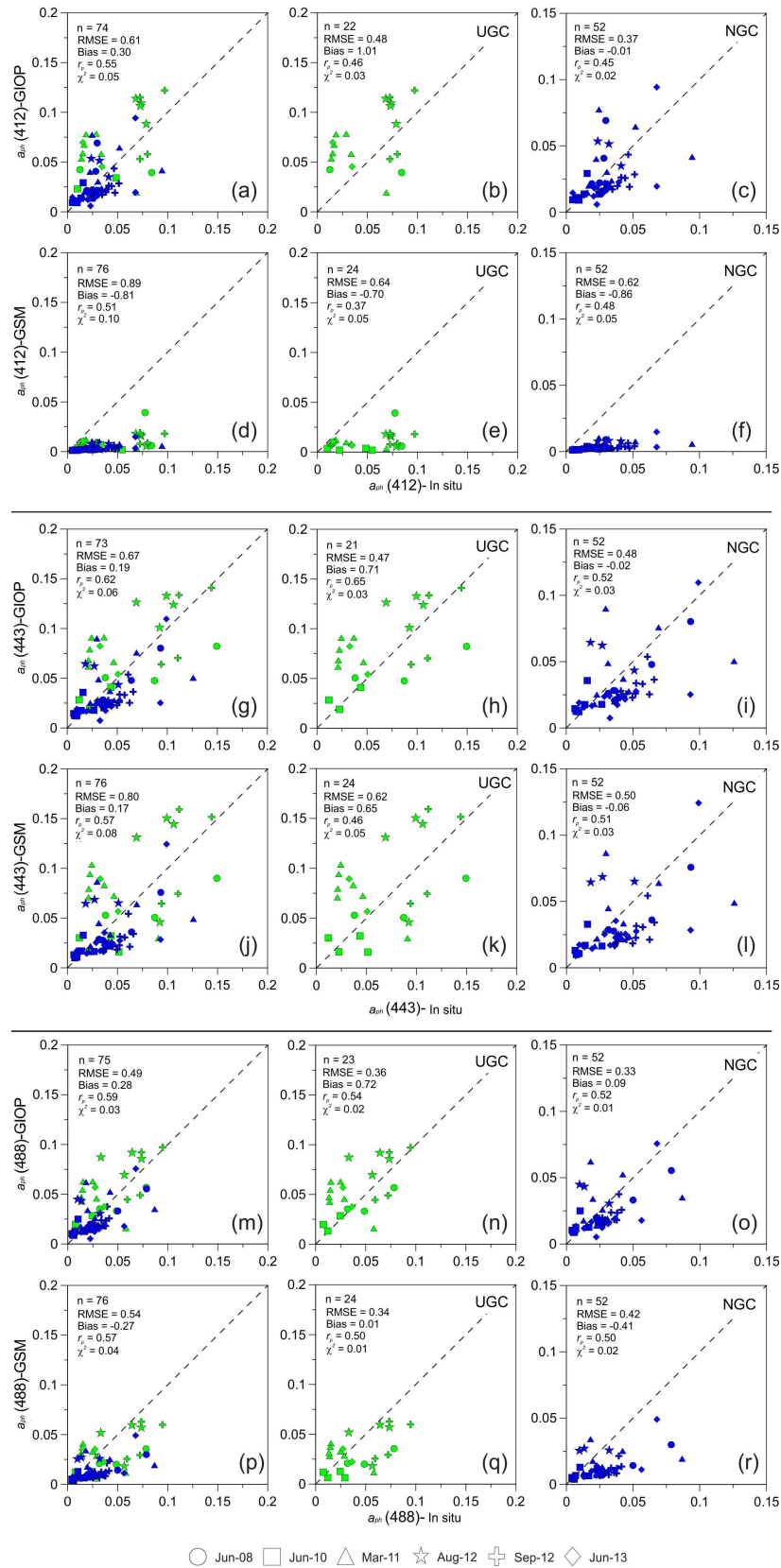


Figure 3. Comparative analysis between in situ and satellite a_{ph} (412, 443, and 488 nm) for GIOP and GSM models, with the statistics Root Mean Square Error (RMSE), bias, r_p , and χ^2 ; the 1:1 line is indicated for reference. The green and blue colors correspond to the UGC and NGC regions, respectively. In the first column (a, d, g, j, m, p) the entire database was used, in the second (b, e, h, k, n, q) only data from UGC, and in the third (c, f, i, l, o, r) only data from NGC.

Taylor diagrams (see Figure 4) confirmed that the $a_{ph}(\lambda)$ derived from GIOP was slightly better than the GSM $a_{ph}(\lambda)$, with higher values of r_p (≈ 0.45) and normalized standard deviations close to 1.0. This, in addition to the underestimation observed in the match-ups independently of the analysis applied (entire dataset and by bio-optical region) and the higher χ^2 value presented by the GSM model, support the conclusion that GIOP better derives $a_{ph}(\lambda)$ values for both bio-optical regions.

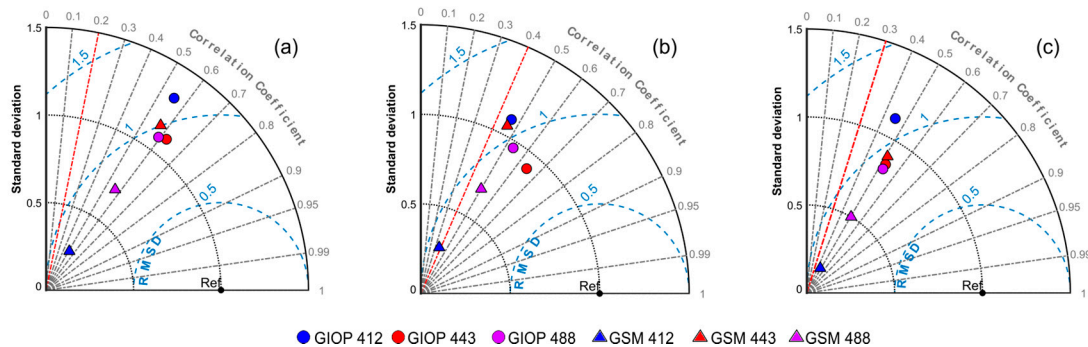


Figure 4. Taylor diagram illustrating the relative performance of the GIOP and GSM algorithms upon reproducing the absorption coefficient a_{ph} (412, 443, and 488 nm). Diagrams represent (a) the entire dataset and data collected in the (b) UGC and (c) NGC. The red line represents the critical value of Pearson's correlation coefficient and indicates the best-model performance.

As previously mentioned, GIOP and GSM use a constant value for $a_{ph}^*(\lambda)$ (i.e., $a_{ph}^*(443) = 0.055 \text{ m}^2 \text{ mgChl}a^{-1}$), which is then scaled according to Chl a concentration to derive $a_{ph}(\lambda)$. Moreover, Chl a is derived from empirical OCx, that is, some of the ocean color band ratio algorithms OC3 or OC4 [38,39]. In this study's data, $a_{ph}^*(443)$ values varied between 0.011 and $0.37 \text{ m}^2 \text{ mgChl}a^{-1}$, where most data were below $0.055 \text{ m}^2 \text{ mgChl}a^{-1}$ (see Figure 5a), with the exception of the June 2013 cruise when values increased to up to $0.37 \text{ m}^2 \text{ mgChl}a^{-1}$. Variability in $a_{ph}^*(\lambda)$ could be associated with changes in pigment composition and cell size [40], which varied among cruises and bio-optical regions [29]. For example, in June 2013 the UGC region was dominated by fucoxanthin, a pigment that indicates the presence of diatoms and larger cells (i.e., microplankton) [41], whereas, in the NGC, zeaxanthin was the major pigment indicating the importance of cyanobacteria and a dominium of small cells (picoplankton) [29]. At the same time, this cruise was the one with the highest number of stations dominated by zeaxanthin (i.e., cyanobacteria) that represented a group characterized by high light absorption efficiency (i.e., high $a_{ph}^*(\lambda)$) [42], which agreed with the study's results (see Figure 5a). Frequency histograms were also generated by region (see Figure 5b,c) to emphasize the differences between them. In the UGC (see Figure 5b), most data were between 0.025 and $0.125 \text{ m}^2 \text{ mgChl}a^{-1}$, whereas, in the NGC, most data were between 0.02 and $0.06 \text{ m}^2 \text{ mgChl}a^{-1}$. Furthermore, the most frequent value (mode) was $0.03 \text{ m}^2 \text{ mgChl}a^{-1}$ in both regions. These results indicated that a change in the default input values used by GSM and GIOP should be considered in addition to a temporal adjustment of the same value in order to improve $a_{ph}(\lambda)$ estimations in the study area.

Another source of error in both algorithms could be the satellite estimation of Chl a (i.e., OCx performance). To evaluate its influence in the $a_{ph}(\lambda)$ calculation, the satellite estimates were compared with in situ measurements (see Figure 6). Results for the entire dataset ($n = 122$) indicated an overestimation of in situ Chl a (bias = 1.72) with a RMSE of 0.45 and a correlation coefficient of 0.76. The positive bias was larger for the NGC and smaller for the UGC.

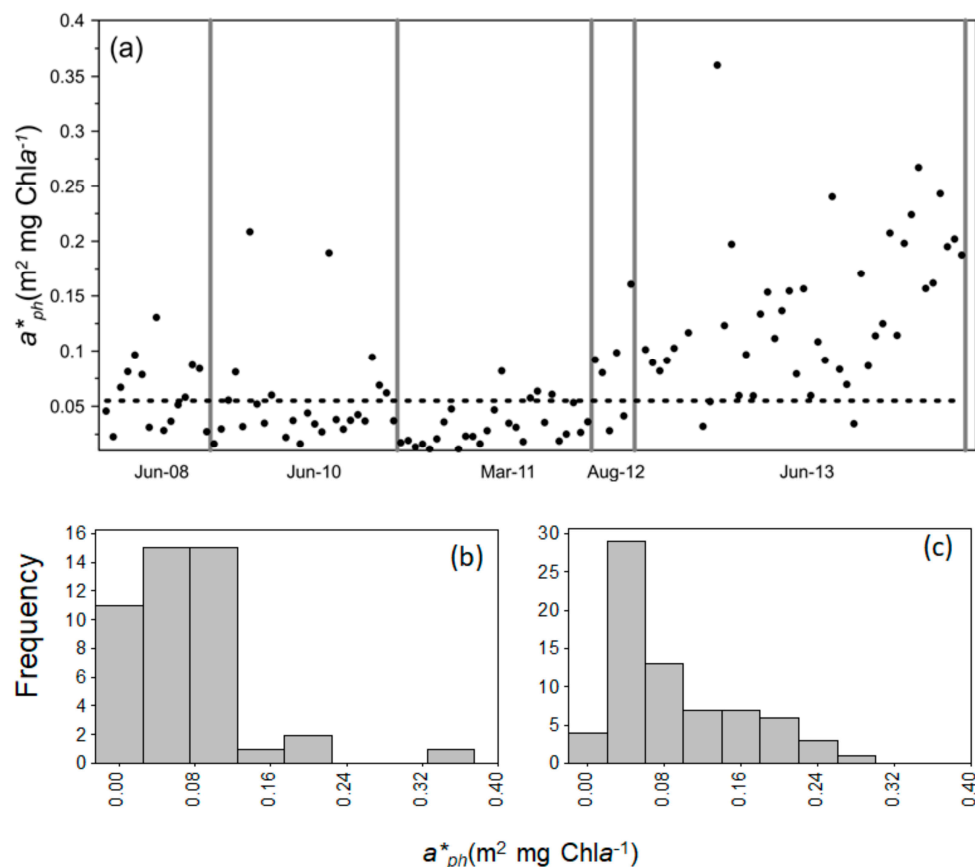


Figure 5. (a) In situ a^*_{ph} (m² mgChla⁻¹) variability for all cruises analyzed in this study, including the value used in GIOP and GSM ($a^*_{ph} = 0.055$ m² mgChla⁻¹, dotted line). Also indicated are the frequency histograms for (b) UGC and (c) NGC.

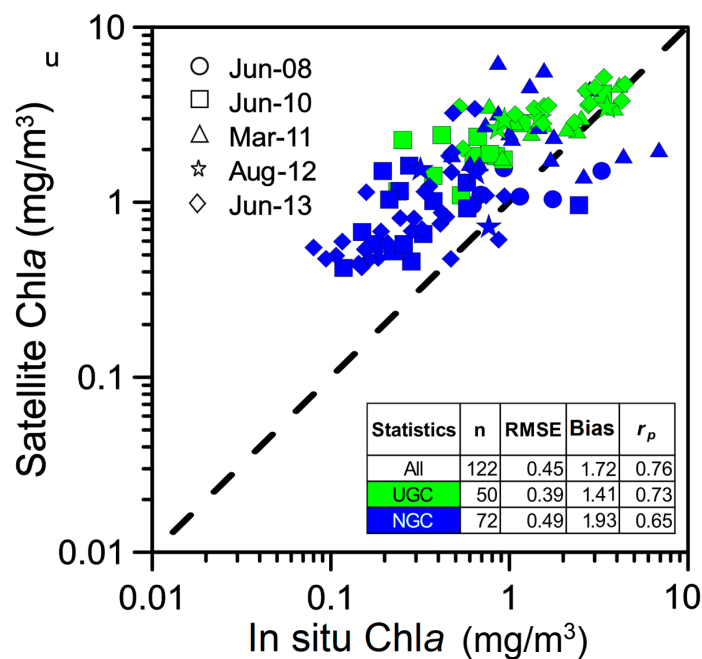


Figure 6. Relationship between in situ chlorophyll data (Chla) and satellite chlorophyll data for the June 2008, June 2010, March 2011, August 2012, and June 2013 cruises, plotted on a logarithmic scale. The dashed line is the one-to-one line. RMSE is computed on log10-transformed data, and bias on original data.

In summary, there was a slight underestimation of $a_{ph}(443)$ in the NGC (GIOP bias = -0.02 , GSM bias = -0.06) related to an underestimation of $a_{ph}^*(443)$ and a strong overestimation of Chla (bias = 1.93). There was a strong overestimation of $a_{ph}(\lambda)$ in the UGC (GIOP bias = 0.71 , GSM bias = 0.65) related to the same underestimation of $a_{ph}^*(443)$ and smaller overestimation of Chla (bias = 1.41). A positive relationship was expected between Chla and $a_{ph}(\lambda)$ [40], i.e., an overestimation of in situ Chla would result in an overestimation of $a_{ph}(\lambda)$. If it is assumed that the same error is associated with $a_{ph}^*(443)$ in both regions, differences between them should be related to Chla. Our results suggest that in the NGC the effect of underestimating $a_{ph}^*(443)$ somewhat compensated the effect of overestimating Chla. In the UGC, on the other hand, the fact that $a_{ph}^*(443)$ was more variable than in the NGC should be taken into consideration, which would explain, at least partly, the inferior performance of both algorithms.

3.2. Absorption Coefficient of Dissolved and Detrital Matter

The total number of a_{dg} (412, 443, and 448) in situ data were 84; however, for the same reasons previously explained (Section 3.1), only 28 match-ups were generated for GIOP and 32 for GSM (see Figure 2b). The difference in the number of data used for GIOP and GSM was due to outliers that were excluded from the analysis. The data used for these analyses are listed in the Supplementary Material (see Table S2). The comparative analysis between the absorption coefficient $a_{dg}(\lambda)$ measured in situ and retrieved by GIOP and GSM was done with the entire dataset and by bio-optical region for wavelengths centered on 412, 443, and 488 nm (see Figure 7). In general, GIOP gave better results than GSM represented by lower RMSE and higher r_p and χ^2 . Irrespective of the algorithm used, the best estimations were at 488 nm, whereas the poorest sensitivity was observed at 412 nm. When comparing algorithm performance in the UGC and the NGC, it was observed that estimations were more accurate in the NGC than in the UGC.

Taylor diagrams indicate that both algorithms were statistically significant ($\alpha = 0.05$) when the analysis was done without distinguishing between bio-optical regions (Figure 8a compared with Figure 8b,c), with higher values of r_p (>0.60) and normalized standard deviations around 0.8 for GIOP and with a higher dispersion for GSM. However, when data was analyzed by region, it was observed that in the UGC, r_p were lower than the critical value (-0.60 and 0.60) for both algorithms, indicating that neither one was able to reproduce the in situ values of $a_{dg}(\lambda)$. In the NGC, r_p were above 0.50 and statistically significant ($r_{calculated} > r_{critical}$, $\alpha = 0.05$).

In conclusion, both GIOP and GSM performed poorly for $a_{dg}(\lambda)$ estimations. In the UGC region, they underestimated the in situ data and, according to r_p , estimations were not statistically accurate. For the NGC region, the situation changed, given that the statistics were slightly better for GIOP than for GSM, with higher r_p values (>0.29), normalized standard deviations close to 1.0, lower values of RMSE, bias close to zero, and the lowest values of χ^2 . This indicates that the algorithm that best derives $a_{dg}(\lambda)$ for the NGC is GIOP.

Because $a_{dg}(\lambda)$ was calculated as the sum of $a_d(\lambda)$ and $a_{CDOM}(\lambda)$, it was considered important to analyze the average spectra of these individual variables for each cruise and bio-optical region. This analysis was conducted by comparing the values of $a_{dg}(\lambda)$ from GIOP and GSM at five wavelengths (412, 443, 448, 555, and 678), specifying the contribution given by detritus ($a_d(\lambda)$) and CDOM ($a_{CDOM}(\lambda)$) to the absorption coefficient $a_{dg}(\lambda)$. The underestimation associated with both algorithms appeared related to those cruises for which the contribution from detritus to $a_{dg}(\lambda)$ was greater than that from CDOM (see Figure 9b–d), independently of the bio-optical region.

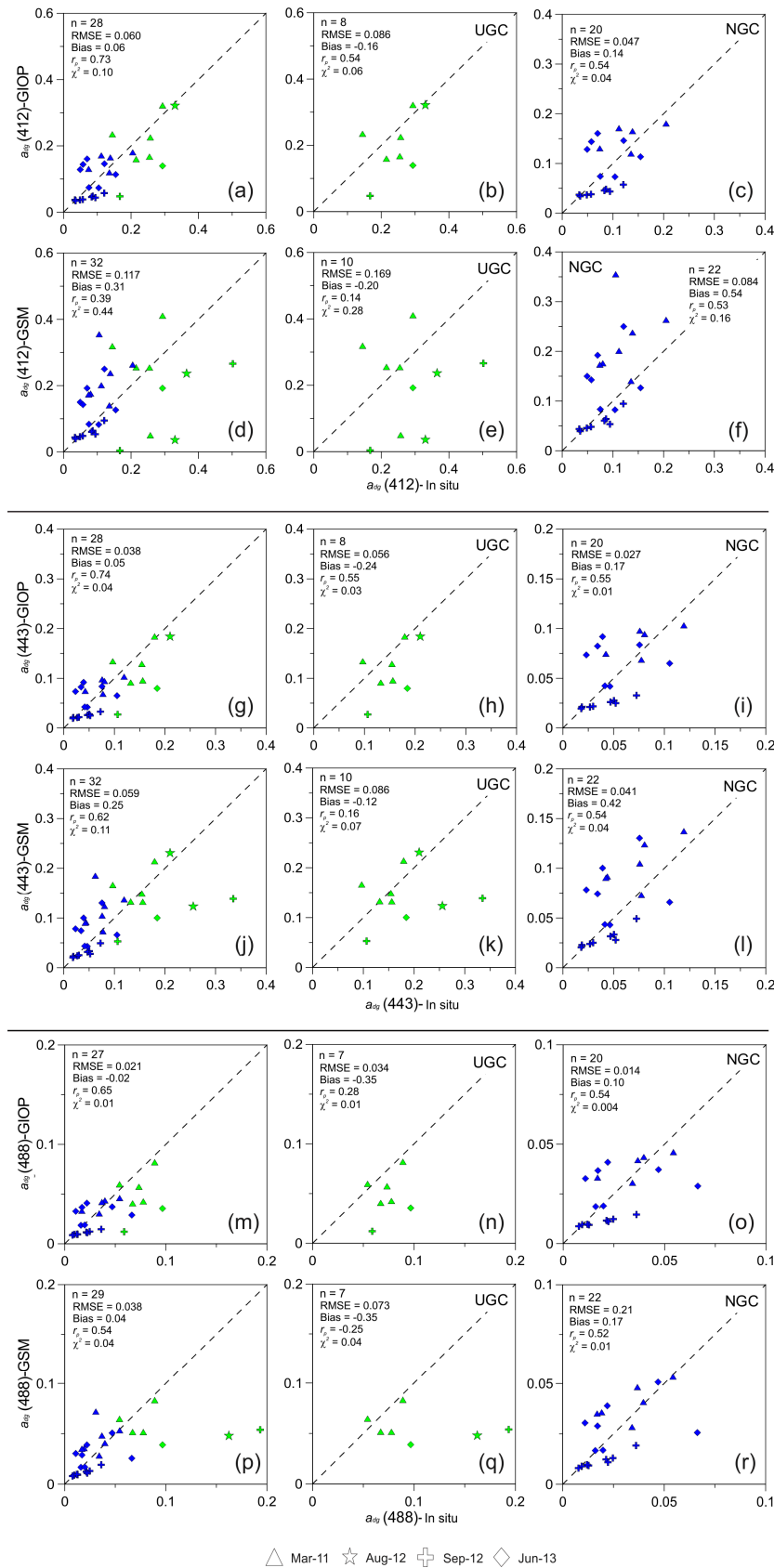


Figure 7. Comparative analysis between in situ and satellite a_{dg} (412, 443, and 448) for the GIOP and GSM algorithms, with statistics Root Mean Square Error (RMSE), bias, r_p , and χ^2 . The 1:1 is indicated for reference. The green and blue colors correspond to the UGC and NGC regions, respectively. In the first column (a, d, g, j, m, p) the entire database was used, in the second (b, e, h, k, n, q) only data from UGC, and in the third (c, f, i, l, o, r) only data from NGC.

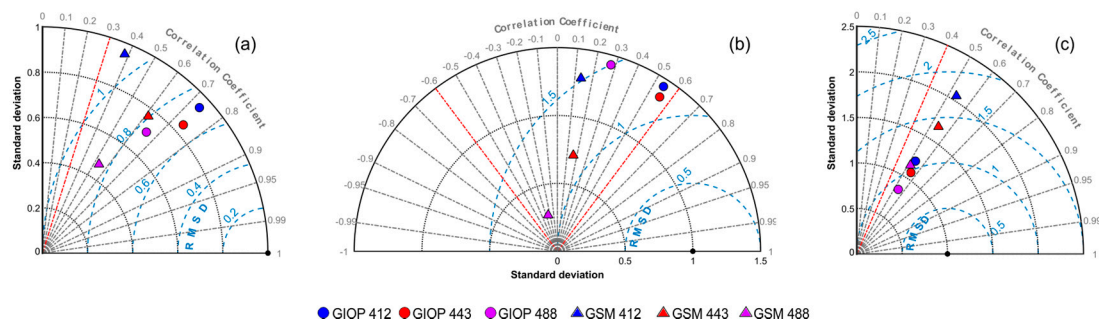


Figure 8. Taylor diagram illustrating the relative performance of the algorithms GIOP and GSM in reproducing the absorption coefficient a_{dg} (412, 443, and 488 nm). Each diagram represents the analysis applied to (a) all of the data and by bio-optical regions (b) UGC and (c) NGC. The dotted red line represents the critical value of Pearson's correlation coefficient.

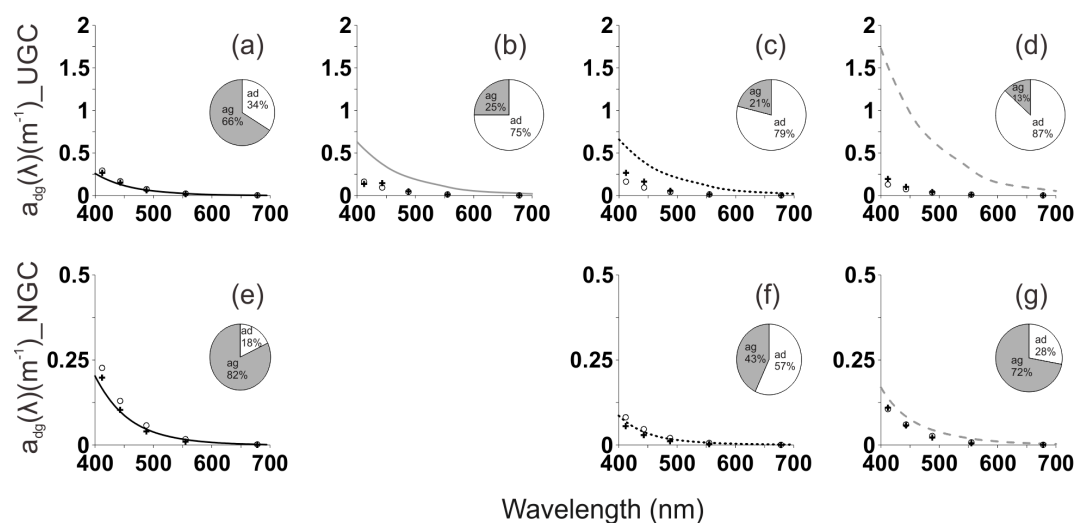


Figure 9. Average spectra of the absorption coefficient of dissolved and detrital matter ($a_{dg}(\lambda)$) calculated for each cruise in the UGC (a–d) and NGC (e–g). The pie chart inside diagrams represents the percentage contribution of detritus (a_d) and chromophoric dissolved organic material (CDOM) (a_g) to $a_{dg}(\lambda)$. Open circles represent GSM $a_{dg}(\lambda)$ values and black crosses represent GIOP $a_{dg}(\lambda)$ values. Note: The August 2012 cruise was represented by a single station and was not included in the figure.

The estimation of $a_{dg}(\lambda)$ by GSM considers an S_{dg} value of 0.0206, whereas GIOP considers a value of 0.018. However, in situ data showed that most values were below 0.018 especially in the UGC where the mode was 0.012, whereas, in the NGC, it was 0.018 (see Figure 9). Lower values of S_{dg} were related with a higher contribution by detritus, as was the case in August 2012, September 2012, and June 2013 in the UGC (see Figure 10). These results suggested that the input value for S_{dg} should be modified for UGC to yield better $a_{dg}(\lambda)$ estimations. After using the in situ S_{dg} as model input, the results were much improved (see Table 4). In the NGC, characterized by a greater dispersion of in situ S_{dg} values, the statistical improvement was much more evident than in the UGC, especially with the GSM algorithm.

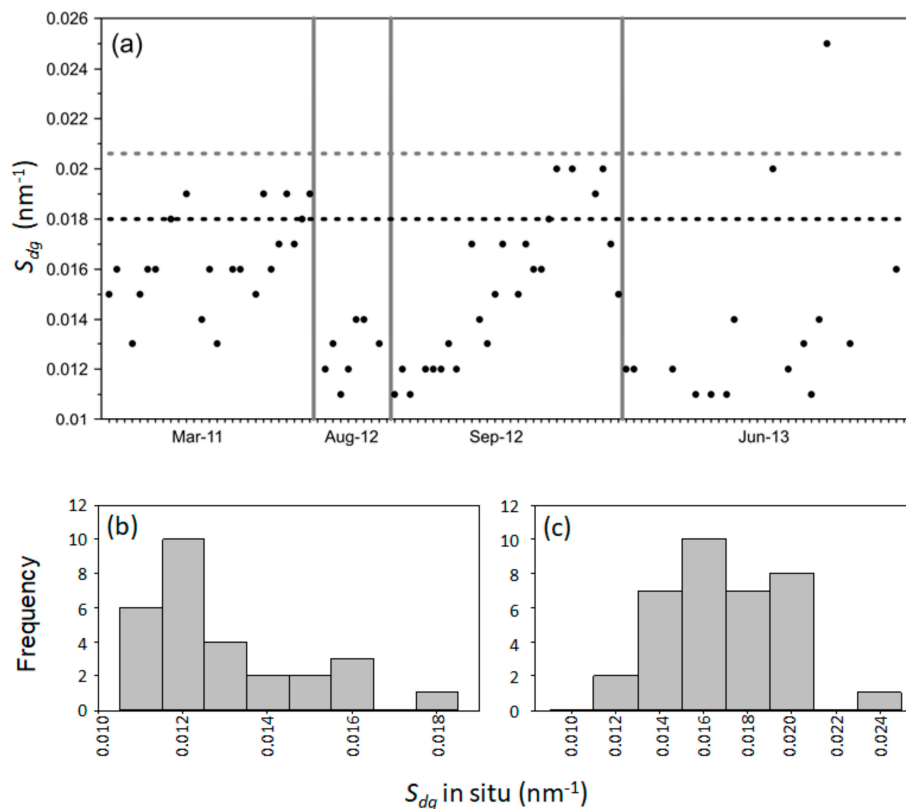


Figure 10. (a) In situ S_{dg} variability for all cruises analyzed in this study, including the value used in GIOP ($S_{dg} = 0.018$, black dotted line) and GSM ($S_{dg} = 0.02061$, gray dotted line). Also indicated are the frequency histograms for (b) UGC and (c) NGC.

Table 4. Comparison between statistics applied to the in situ absorption coefficient $a_{dg}(\lambda)$ and the outputs of the models in their default configurations (GIOP, GSM), and the outputs after adjustment with the in situ S_{dg} values (GIOP *, GSM *). The lowest values of RMSE and Least squares are indicated in bold letters.

λ		N		$SD_{In\ situ}$		$SD_{Satellite}$		RMSE		Bias		Least Squares	
		GIOP	GIOP *	GIOP	GIOP *	GIOP	GIOP *	GIOP	GIOP *	GIOP	GIOP *	GIOP	GIOP *
UGC	412	11	11	0.19	0.19	0.09	0.13	2.45	2.34	−0.32	−0.26	0.75	0.69
	443	11	11	0.14	0.14	0.05	0.05	1.77	1.57	−0.39	−0.19	0.39	0.31
	488	11	8	0.09	0.10	0.02	0.01	1.18	1.04	−0.51	−0.42	0.18	0.13
NGC	412	26	26	0.14	0.14	0.09	0.08	2.25	2.06	0.23	0.35	0.63	0.53
	443	26	26	0.09	0.09	0.05	0.04	1.43	1.32	0.25	0.25	0.26	0.22
	488	26	26	0.05	0.05	0.02	0.02	0.76	0.72	0.19	0.02	0.07	0.06
λ		GSM	GSM *	GSM	GSM *	GSM	GSM *	GSM	GSM *	GSM	GSM *	GSM	GSM *
UGC	412	10	5	0.10	0.08	0.13	0.14	1.51	0.57	−0.20	−0.05	0.14	0.72
	443	10	7	0.07	0.08	0.05	0.09	0.76	0.48	−0.12	0.13	0.16	0.68
	488	7	5	0.05	0.06	0.01	0.04	0.54	0.16	−0.35	0.09	−0.25	0.88
NGC	412	22	17	0.04	0.04	0.09	0.10	1.12	1.02	0.54	0.41	0.53	0.59
	443	22	18	0.03	0.03	0.05	0.06	0.55	0.67	0.42	0.60	0.54	0.67
	488	22	16	0.02	0.01	0.02	0.04	0.21	0.34	0.17	0.51	0.52	0.79

4. Conclusions

In this study, a statistical analysis was carried out to compare the performance of two semi-analytical algorithms (GIOP and GSM) to retrieve absorption coefficients in regions characterized by different bio-optical properties, namely the UGC and the NGC. GIOP was a better estimator for $a_{ph}(\lambda)$ than GSM, independently of the bio-optical region. Both algorithms, however, underestimated

in situ values (negative bias) in the NGC, whereas they overestimated (positive bias) in the UGC. One possible source of error was the constant $a_{ph}^*(443)$ value used by GSM and GIOP ($0.055 \text{ m}^2 \text{ mgChl}a^{-1}$) that was higher than the most frequent value observed in the study's data ($0.03 \text{ m}^2 \text{ mgChl}a^{-1}$). Other uncertainties were associated with the satellite Chl a estimation, which overestimated the in situ Chl a . Furthermore, GIOP gave better results for the $a_{dg}(\lambda)$ estimation than GSM, especially in the NGC. The most important observation was that the underestimation associated with both algorithms was obtained for cruises during which the contribution from detritus to $a_{dg}(\lambda)$ was greater than that from CDOM, independently of the bio-optical region. Indeed, the spectral slope S_{dg} was identified as an important term for the accurate estimation of $a_{dg}(\lambda)$, and the study's results indicated that using a fixed input value was not adequate. Observations have to be taken in account for future improvements of this type of model in this region and other optically complex waters. The evaluation confirms the lack of generality of algorithms like GIOP and GSM, whose reflectance model is too simplified to capture expected variability. Finally, a greater monitoring effort is suggested in the study area regarding the collection of in situ reflectance data, which would allow explaining the effects that detritus and CDOM have on the semi-analytical reflectance inversions, as well as isolating the possible influence of the atmosphere on the satellite-derived water reflectance and Chl a .

Supplementary Materials: The following are available online at <http://www.mdpi.com/2072-4292/10/9/1443/s1>, In Tables S1 and S2 there is the data used for the analyses presented in this work.

Author Contributions: S.P.B.-T. and A.G.-S. conceived and designed the data processing and analyses; E.S.d.-A. was responsible of in situ data sampling, participated in statistical analyses and collaborated throughout the entire process with ideas, corrections, and advisory sessions; J.T. participated in data processing (application of GIOP and GSM) and, with R.F., provided suggestions and courses of action, and they both contributed to the writing and editing of the manuscript.

Funding: This research was funded by projects SIMAC-CONACYT, SIMAC-2000107017; CICESE: Ecological monitoring of the Upper Gulf of California" (PANGAS-Packard Foundation); IPN-CICIMAR: SIP 1721, 20160514-CONACYT: 236864. The Secretariat of the Mexican Navy and R/V Francisco de Ulloa (CICESE) supported the cruises.

Acknowledgments: The first author received support from CONACyT (Mexican Council of Science) through a Ph.D. scholarship (No. 384224) and during August–December 2018 from the Inter-American Institute for Global Change Research (IAI) through the grant IAI-CRN3094. The National Aeronautics and Space Administration supported the work of R. Frouin and J. Tan under grants NNX14AM3G and NNX14AQ46A. We thank all the students from the Phytoplankton Ecology Team of the Faculty of Marine Science that participated in cruises and sampling procedures. The authors gratefully acknowledge the comments of anonymous reviewers.

Conflicts of Interest: The authors declare no conflict of interest. The funding sponsors had no role in the design of the study; in the collection, analyses, or interpretation of data; in the writing of the manuscript, and in the decision to publish the results.

References

1. McClain, C.R.; Cleave, M.L.; Feldman, G.C.; Gregg, W.W.; Hooker, S.B.; Kuring, N. Science Quality SeaWiFS Data for Global Biosphere Research. Available online: https://rsg.pml.ac.uk/staff/tjsm/sea_tech.html (accessed on 18 August 2017).
2. McClain, C.R.; Christian, J.R.; Signorini, S.R.; Lewis, M.R.; Asanuma, I.; Turk, D.; Dupouy-Douchement, C. Satellite ocean-color observations of the tropical Pacific Ocean. *Deep Sea Res. Part II Top. Stud. Oceanogr.* **2002**, *49*, 2533–2560. [CrossRef]
3. Gregg, W.W.; Conkright, M.E.; Ginoux, P.; O'Reilly, J.E.; Casey, N.W. Ocean primary production and climate: Global decadal changes. *Geophys. Res. Lett.* **2003**, *30*, 1809. [CrossRef]
4. Behrenfeld, M.J.; Boss, E.; Siegel, D.A.; Shea, D.M. Carbon-based ocean productivity and phytoplankton physiology from space. *Glob. Biogeochem. Cycles* **2005**, *19*, GB1006. [CrossRef]
5. Yoder, J.; Kennelly, M. What Have We Learned About Ocean Variability from Satellite Ocean Color Imagers? *Oceanography* **2006**, *19*, 152–171. [CrossRef]
6. Garver, S.A.; Siegel, D.A. Inherent optical property inversion of ocean color spectra and its biogeochemical interpretation: 1. Time series from the Sargasso Sea. *J. Geophys. Res. Oceans* **1997**, *102*, 18607–18625. [CrossRef]

7. Lee, Z.; Carder, K.L.; Steward, R.G.; Peacock, T.G.; Davis, C.O.; Patch, J.S. An empirical algorithm for light absorption by ocean water based on color. *J. Geophys. Res. Oceans* **1998**, *103*, 27967. [[CrossRef](#)]
8. Carder, K.L.; Chen, F.R.; Lee, Z.P.; Hawes, S.K.; Kamykowski, D. Semianalytic Moderate-Resolution Imaging Spectrometer algorithms for chlorophyll a and absorption with bio-optical domains based on nitrate-depletion temperatures. *J. Geophys. Res. Oceans* **1999**, *104*, 5403–5421. [[CrossRef](#)]
9. Morel, A.; Maritorena, S. Bio-optical properties of oceanic waters: A reappraisal. *J. Geophys. Res. Oceans* **2001**, *106*, 7163–7180. [[CrossRef](#)]
10. Lee, Z.-P.; Darecki, M.; Carder, K.L.; Davis, C.O.; Stramski, D.; Rhea, W.J. Diffuse attenuation coefficient of downwelling irradiance: An evaluation of remote sensing methods. *J. Geophys. Res. Oceans* **2005**, *110*. [[CrossRef](#)]
11. Lee, Z.-P.; Du, K.; Arnone, R.; Liew, S.; Penta, B. Penetration of solar radiation in the upper ocean: A numerical model for oceanic and coastal waters. *J. Geophys. Res. Oceans* **2005**, *110*. [[CrossRef](#)]
12. Hu, C.; Lee, Z.; Muller-Karger, E.; Carder, L.; Walsh, J.J. Ocean color reveals phase shift between marine plants and yellow substance. *IEEE Geosci. Remote Sens. Lett.* **2006**, *3*, 262–266. [[CrossRef](#)]
13. Capuzzo, E.; Painting, S.J.; Forster, R.M.; Greenwood, N.; Stephens, D.T.; Mikkelsen, O.A. Variability in the sub-surface light climate at ecohydrodynamically distinct sites in the North Sea. *Biogeochemistry* **2013**, *113*, 85–103. [[CrossRef](#)]
14. Haraldsson, M.; Tönnesson, K.; Tiselius, P.; Thingstad, T.; Aksnes, D. Relationship between fish and jellyfish as a function of eutrophication and water clarity. *Mar. Ecol. Prog. Ser.* **2012**, *471*, 73–85. [[CrossRef](#)]
15. Siegel, D.A.; Behrenfeld, M.J.; Maritorena, S.; McClain, C.R.; Antoine, D.; Bailey, S.W.; Bontempi, P.S.; Boss, E.S.; Dierssen, H.M.; Doney, S.C.; et al. Regional to global assessments of phytoplankton dynamics from the SeaWiFS mission. *Remote Sens. Environ.* **2013**, *135*, 77–91. [[CrossRef](#)]
16. Brewin, R.J.; Sathyendranath, S.; Müller, D.; Brockmann, C.; Deschamps, P.-Y.; Devred, E.; Doerffer, R.; Fomferra, N.; Franz, B.; Grant, M. The Ocean Colour Climate Change Initiative: III. A round-robin comparison on in-water bio-optical algorithms. *Remote Sens. Environ.* **2013**, *162*, 271–294. [[CrossRef](#)]
17. Mitchell, B.G.; Kahru, M.; Wieland, J.; Stramska, M.; Mueller, J.L. Determination of spectral absorption coefficients of particles, dissolved material and phytoplankton for discrete water samples. *Ocean Opt. Protoc. Satell. Ocean Color Sens. Valid. Revis.* **2002**, *3*, 231–257.
18. Kirk, J.T. *Light and Photosynthesis in Aquatic Ecosystems*; Cambridge University Press: Cambridge, MA, USA, 1994.
19. Lee, Z.P. *Remote Sensing of Inherent Optical Properties: Fundamentals, Tests of Algorithms, and Applications*; International Ocean-Colour Coordinating Group: Dartmouth, NS, Canada, 2006; Volume 5.
20. Sathyendranath, S. *Remote Sensing of Ocean Colour in Coastal, and Other Optically-Complex*; IOCCG Report 3; IOCCG: Dartmouth, NS, Canada, 2000; p. 3.
21. Maritorena, S.; Siegel, D.A.; Peterson, A.R. Optimization of a semianalytical ocean color model for global-scale applications. *Appl. Opt.* **2002**, *41*, 2705–2714. [[CrossRef](#)] [[PubMed](#)]
22. Werdell, P.J.; Franz, B.A.; Bailey, S.W.; Feldman, G.C.; Boss, E.; Brando, V.E.; Dowell, M.; Hirata, T.; Lavender, S.J.; Lee, Z.; et al. Generalized ocean color inversion model for retrieving marine inherent optical properties. *Appl. Opt.* **2013**, *52*, 2019–2037. [[CrossRef](#)] [[PubMed](#)]
23. Gordon, H.R.; Brown, O.B.; Evans, R.H.; Brown, J.W.; Smith, R.C.; Baker, K.S.; Clark, D.K. A semianalytic radiance model of ocean color. *J. Geophys. Res. Atmos.* **1988**, *93*, 10909–10924. [[CrossRef](#)]
24. Lee, Z.; Carder, K.L.; Arnone, R.A. Deriving inherent optical properties from water color: A multiband quasi-analytical algorithm for optically deep waters. *Appl. Opt.* **2002**, *41*, 5755–5772. [[CrossRef](#)] [[PubMed](#)]
25. Lee, Z.; Lubac, B.; Werdell, J.; Arnone, R. *An Update of the Quasi-Analytical Algorithm (QAA_v5)*; IOCCG: Dartmouth, NS, Canada, 2009; pp. 1–9.
26. Lee, Z.; Carder, K.L.; Mobley, C.D.; Steward, R.G.; Patch, J.S. Hyperspectral remote sensing for shallow waters. I. A semianalytical model. *Appl. Opt.* **1998**, *37*, 6329–6338. [[CrossRef](#)] [[PubMed](#)]
27. Lavín, M.F.; Marinone, S.G. An overview of the physical oceanography of the Gulf of California. In *Nonlinear Processes in Geophysical Fluid Dynamics*; Velasco Fuentes, O.U., Sheibaum, J., Ochoa, J., Eds.; Springer: Dordrecht, The Netherlands, 2003; pp. 173–204.
28. Bastidas-Salamanca, M.; González-Silvera, A.; Millán-Núñez, R.; Santamaría-del-Ángel, E.; Frouin, R. Bio-Optical Characteristics of the Northern Gulf of California during June 2008. *Int. J. Oceanogr.* **2014**, *13*. [[CrossRef](#)]

29. Betancur-Turizo, S.P.; González-Silvera, A.G.; Santamaría-Del-Ángel, E.; Millán-Núñez, R.; Millán-Núñez, E.; García-Nava, H.; Godínez, V.M.; Sánchez-Velasco, L. Variability in the Light Absorption Coefficient by Phytoplankton, Non-Algal Particles and Colored Dissolved Organic Matter in the Northern Gulf of California. *Open J. Mar. Sci.* **2018**, *8*, 20–37. [[CrossRef](#)]
30. Argote, M.L.; Amador, A.; Lavín, M.F.; Hunter, J.R. Tidal dissipation and stratification in the Gulf of California. *J. Geophys. Res. Oceans* **1995**, *100*, 16103–16118. [[CrossRef](#)]
31. Hooker, S.B.; Clementson, L.; Thomas, C.S.; Schlüter, L. The HPLC Method, Chapter 6. In *The Fifth SeaWiFS HPLC Analysis Round-Robin Experiment (SeaHARRE-5)*; NASA Technical Memorandum: Lanham, MD, USA, 2012; pp. 63–72.
32. Werdell, P.J.; Franz, B.A.; Bailey, S.W.; Harding, L.W., Jr.; Feldman, G.C. Approach for the long-term spatial and temporal evaluation of ocean color satellite data products in a coastal environment. *SPIE* **2007**, *6680*, 66800G.
33. Maritorena, S.; Siegel, D.A. Chapter 11: The GSM semi-analytical bio-optical model. *Remote Sens. Inherent Opt. Prop. Fundam. Tests Algorithms Appl.* **2006**, 73–79.
34. Santamaría-del-Ángel, E.; Millán-Núñez, R.; González-Silvera, A.; Cajal-Medrano, R. Comparison of In Situ and Remotely-Sensed Chl-a concentrations: A Statistical Examination of the Match-up Approach. In *Handbook of Satellite Remote Sensing Image Interpretation: Applications for Marine Living Resources Conservation and Management*; EU PRESPO Project: Wittibrecht, Germany, 2010; pp. 221–238.
35. Zar, H.H. *Biostatistical Analysis*, 4th ed.; Prentice Hall: Upper Saddle River, NJ, USA, 1999.
36. Lee, Y.J.; Matrai, P.A.; Friedrichs, M.A.; Saba, V.S.; Aumont, O.; Babin, M.; Buitenhuis, E.T.; Chevallier, M.; De Mora, L.; Dessert, M. Net primary productivity estimates and environmental variables in the Arctic Ocean: An assessment of coupled physical-biogeochemical models. *J. Geophys. Res. Oceans* **2016**, *121*, 8635–8669. [[CrossRef](#)]
37. Taylor, K.E. Summarizing multiple aspects of model performance in a single diagram. *J. Geophys. Res. Atmos.* **2001**, *106*, 7183–7192. [[CrossRef](#)]
38. O'Reilly, J.E.; Maritorena, S.; Mitchell, B.G.; Siegel, D.A.; Carder, K.L.; Garver, S.A.; Kahru, M.; McClain, C. Ocean color chlorophyll algorithms for SeaWiFS. *J. Geophys. Res. Oceans* **1998**, *103*, 24937–24953. [[CrossRef](#)]
39. O'Reilly, J.E.; Maritorena, S.; Siegel, D.A.; O'Brien, M.C.; Toole, D.; Mitchell, B.G.; Kahru, M.; Chavez, F.P.; Strutton, P.; Cota, G.F. Ocean color chlorophyll algorithms for SeaWiFS, OC2, and OC4: Version 4. *SeaWiFS Postlaunch Calibration Valid. Anal.* **2000**, *3*, 9–23.
40. Bricaud, A.; Claustre, H.; Ras, J.; Oubelkheir, K. Natural variability of phytoplanktonic absorption in oceanic waters: Influence of the size structure of algal populations. *J. Geophys. Res. Oceans* **2004**, *109*. [[CrossRef](#)]
41. Jeffrey, S.W.; Mantoura, R.F.C.; Wright, S.W. *Phytoplankton Pigments in Oceanography: Guidelines to Modern Methods*; UNESCO Publishing: Paris, France, 1997; ISBN 978-92-3-103275-2.
42. Millán-Núñez, E.; Sieracki, M.E.; Millán-Núñez, R.; Lara-Lara, J.R.; Gaxiola-Castro, G.; Trees, C.C. Specific absorption coefficient and phytoplankton biomass in the southern region of the California Current. *Deep Sea Res. Part II Top. Stud. Oceanogr.* **2004**, *51*, 817–826. [[CrossRef](#)]

